Hindawi Publishing Corporation
Journal of Nanomaterials
Volume 2012, Article ID 469143, 7 pages
doi:10.1155/2012/469143

Research Article

Top-Down Processing of $NaNbO_3$ Nanopowder

Jurij Koruza,[1,2] Barbara Malič,[1] Oleksandr Noshchenko,[1] and Marija Kosec[1,2]

[1] *Electronic Ceramics Department, Jožef Stefan Institute, Jamova cesta 39, 1000 Ljubljana, Slovenia*
[2] *Centre of Excellence NAMASTE, Jamova cesta 39, 1000 Ljubljana, Slovenia*

Correspondence should be addressed to Jurij Koruza, jurij.koruza@ijs.si

Received 23 February 2012; Accepted 5 April 2012

Academic Editor: Sergio J. Mejía-Rosales

We report the processing of $NaNbO_3$ nanopowder by combining the solid-state synthesis and subsequent milling in the agitator bead mill. The effect of different rotation speeds of the agitator shaft on the comminution process was followed by laser granulometry. The morphology and specific surface area of the powders were investigated by scanning electron microscopy and the N_2 adsorption method, respectively. With the optimized milling parameters, we obtained $NaNbO_3$ nanoparticles with an average size of 25 nm and a narrow particle size distribution. The result is comparable to other processing techniques, such as solution-based chemical routes or mechanochemical synthesis; however, the presented method does not require any complicated processing and it can be easily upscaled to yield large quantities of the $NaNbO_3$ nanopowder. Furthermore, the compaction behaviour of the obtained nanopowder was investigated, and a compaction-response diagram was constructed revealing good compactability of the powder. The green compacts, isostatically pressed at 740 MPa, had a relative density of 70% and a narrow pore size distribution with an average pore radius of 4 nm.

1. Introduction

Antiferroelectric materials have gained increased attention due to their large energy storage capacity, required for high-performance capacitors [1], and a large volume change accompanying the field-induced phase transition, which may be used in high-strain actuator and transducer applications [2]. Lead zirconate ($PbZrO_3$) is a prototype antiferroelectric [3, 4]; however, due to increased environmental concerns [5], lead-free antiferroelectrics, such as sodium niobate ($NaNbO_3$), are considered [6]. The phase transition behaviour of $NaNbO_3$ is quite complicated [7]. Beside the temperature and electric-field-induced phase transitions, size-induced phase transition phenomena have been recently observed [8, 9]. In order to investigate the effect of the particle/grain sizes on the polymorphism, and consequently on the functional properties, dense $NaNbO_3$ ceramics with a wide grain size range should be prepared. A necessary condition for the preparation of ultrafine-grained ceramics is the $NaNbO_3$ nanopowder.

Nobre et al. prepared $NaNbO_3$ nanoparticles by the Pechini route and calcination of the precursor at 700°C for 5 h. The powder had the particle size of around 60 nm, as determined by the Brunauer-Emmet-Teller (BET) method [10]. Lanfredi et al. prepared the $NaNbO_3$ nanoparticles from the solution of an oxalatoniobium complex, sodium nitrate, oxalic acid, and ammonium hydroxide. The particle size of the powder, obtained by calcining the precursor at 900°C for 5 h, was 85 nm, as calculated from the X-ray diffraction (XRD) data by the Sherrer equation. However, some impurities could be observed in the XRD pattern [11]. In both studies, dense $NaNbO_3$ ceramics were obtained after sintering at lower temperatures than usually needed for the solid-state synthesized powder, which was connected to the small particle size and to a high concentration of defects, such as oxygen vacancies. The latter were presumably created due to the incomplete oxidation of organic precursors. In 2005, Pithan et al. introduced a microemulsion-mediated hydrolytic decomposition of a mixed-alkoxide solution, followed by Soxhlet extraction, and subsequent calcining at

400°C to prepare the nanopowder with the particle size of a few 10 nm as observed by scanning electron microscopy (SEM) and the BET size of a few 100 nm [12].

Solution-based chemical routes, applied to prepare $NaNbO_3$ nanopowders, suffer various deficiencies, such as complicated processing, small product yield, difficult upscaling, and sometimes difficulties in a complete removal of residual carbon. In addition, they typically require additional calcination steps to obtain the crystalline product.

An alternative approach was introduced by Rojac et al. who prepared the $NaNbO_3$ nanopowder by mechanochemical synthesis [13]. After 40 h of high-energy milling of Na_2CO_3 and Nb_2O_5 in a planetary mill, the product consisted of agglomerates of 100–300 nm in size, while the crystallites were in the range of 10–20 nm, as determined from the transmission electron microscope images. The process however introduced impurities in the powder due to wear of the ZrO_2 milling vial and balls.

The aim of the present work was to establish a simple and effective processing route for the preparation of $NaNbO_3$ nanopowder by combining conventional and well established ceramic processing techniques, such as the solid-state synthesis of submicron-sized powder [9] and subsequent efficient milling to nanorange in an agitator bead mill. The influences of the milling time and different rotation speeds of the agitator shaft were followed by measurements of the particle size and size distribution and specific surface area. The optimization of the process resulted in a successful preparation of $NaNbO_3$ nanopowder. Furthermore, the nanopowder was isostatically pressed between 250 MPa and 740 MPa and its compaction-response diagram was constructed.

2. Experimental Work

The $NaNbO_3$ powder was prepared by solid-state synthesis from the high-purity Nb_2O_5 (99.9%, Sigma-Aldrich, Taufkirchen, Germany) and mechanically activated Na_2CO_3 (anhydrous 99.9+%, Chempur, Karlsruhe, Germany). The submicron-sized starting powders were mixed in a stoichiometric ratio and homogenized in a planetary mill (Fritsch Pulverisette 4 Vario-Mill, Fritsch GmbH, Idar-Oberstein, Germany) for 4 h, using a zirconia vial and balls, and acetone as the liquid medium (p. A., AppliChem, Darmstadt, Germany). After drying, the powder mixture was pressed into pellets and calcined twice in a closed alumina crucible at 700°C for 4 h with intermediate milling. The product was crushed in an agate mortar and milled in a planetary mill for 4 h, as described above. The particle size distributions of the powders were determined from the area distribution, measured by a static light-scattering granulometer (Microtrac S3500 Particle Size Analyzer, Montgomeryville, PA, USA). The phase purity of the obtained powder was analysed by a PANalytical X'Pert PRO MPD diffractometer equipped with a graphite monochromator (Almelo, The Netherlands), and the material was found to be single phase, since all the peaks could be described with the crystallographic card of the orthorhombic $NaNbO_3$ (Figure 1) [14]. A detailed description of the synthesis and phase analysis can be found elsewhere [9].

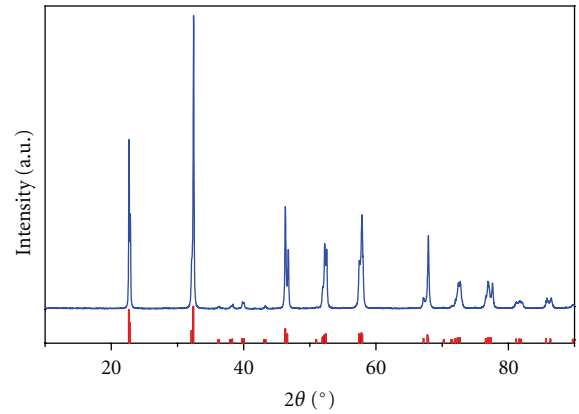

Figure 1: XRD pattern of the solid-state synthesis prepared $NaNbO_3$ (blue line). All the peaks could be described with the crystallographic card of the orthorhombic $NaNbO_3$ (red tick marks).

For milling the $NaNbO_3$ to nanorange, we used the Mini-Cer agitator bead mill (Netzsch Feinmahltechnik GmbH, Selb, Germany), where the grinding medium is accelerated in the chamber by an agitator shaft. Prior milling the as-synthesized powder was dispersed in isopropyl alcohol (p. A., AppliChem, Darmstadt, Germany) in an ultrasonic bath. The suspension was fed through the grinding chamber by a peristaltic hose pump (Verderlab, Haan, Germany), and zirconia beads with a diameter of 0.5 mm (Tosoh Corporation, Tokyo, Japan) were used as the grinding medium. The milling process was followed by the granulometer. The particle size distributions are described with the 90% particle size limit (d_{90}), 50% particle size limit (d_{50}, median value), and 10% particle size limit (d_{10}).

The powder morphology was investigated by a field emission scanning electron microscope (FE-SEM JSM-7600F, Jeol, Tokyo, Japan) with an operating voltage of 5 kV, while the specific surface area was analysed using the N_2 adsorption BET method (NOVA 2200E, Quantachrome Instruments, Boynton Beach, FL, USA). The BET equivalent particle diameters were calculated by the following equation:

$$d_{\mathrm{BET}} = \frac{\psi_A/\psi_V}{S_M \cdot \rho_t}, \tag{1}$$

where S_M is the specific surface area, ρ_t is the theoretical density of $NaNbO_3$ (4.55 g/cm^3 [14]), and ψ_A/ψ_V is the shape factor ratio, for which a value of 6 was assumed [15].

The compaction behaviour of the powders was studied by uniaxial pressing the pellets with a pressure of 100 MPa and subsequently isostatically with pressures ranging from 250 MPa to 740 MPa. The relative densities were calculated from the dimensions and mass of the sample.

The pore size measurements of the compacted pellets were performed using the N_2 sorption equipment described above. The samples were dried at 250°C for 4 h and subsequently degassed at 200°C for 2 h prior to the measurement. The pore size distributions were calculated from the desorption curves using the method proposed by Barrett, Joyner, and Halenda (BJH) [16].

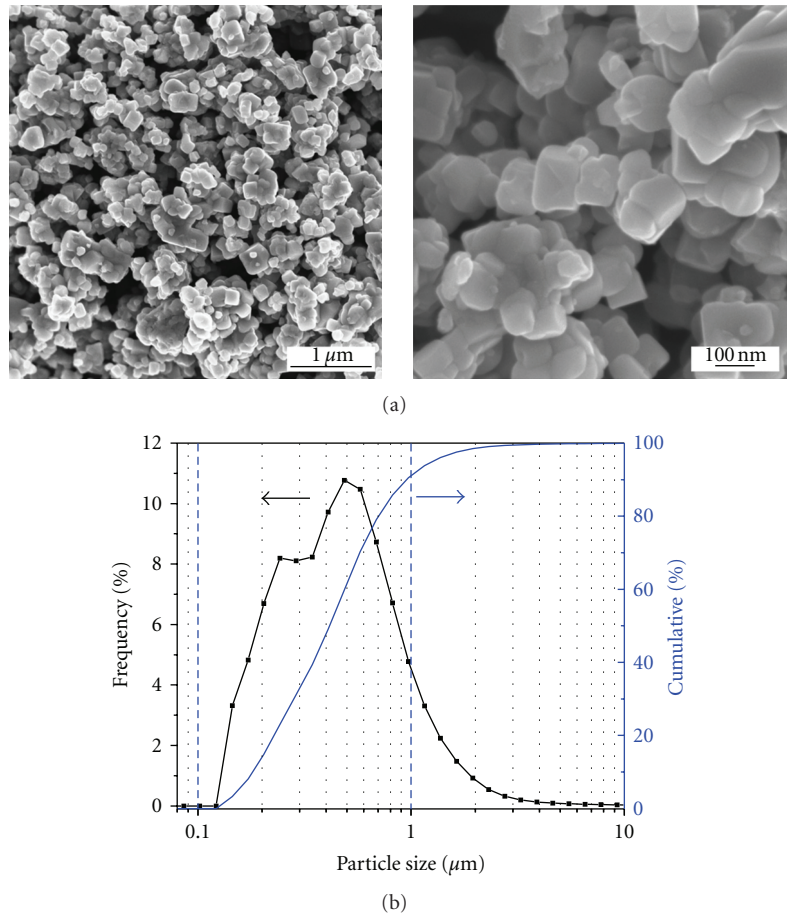

Figure 2: The reference-NN powder prepared by the solid-state synthesis and milled in a planetary mill for 4 h: (a) FE-SEM images and (b) particle size distribution, as measured by laser granulometry.

3. Results and Discussion

The FE-SEM images of the $NaNbO_3$ powder, obtained after the solid-state synthesis and subsequent milling in a planetary mill, are presented in Figure 2(a). This powder is further-on denoted as "reference-NN." The estimated primary particle size was around 200–300 nm; however, some agglomerates of around 400–700 nm could be observed. This was confirmed by the granulometric measurement (Figure 2(b)), with two maxima at around 150–200 nm and 400–500 nm, attributed to the primary particles and to the agglomerates, respectively. The milling in the planetary mill after the calcination obviously failed to break strong agglomerates, created during the calcination process.

In order to prepare the $NaNbO_3$ nanopowder, we milled the reference-NN powder in the agitator bead mill. Different rotation speeds of the agitator shaft, that is, 1000 rpm, 1500 rpm, and 2000 rpm, were applied. The milled powders are denoted as "nano-NN-1000," "nano-NN-1500," and "nano-NN-2000," respectively. The milling process was followed by measuring the particle size distributions by laser granulometry which allowed a quick evaluation of the milling process, since the samples could be rapidly transported in the form of a suspension directly from the mill to the granulometer. The results of the milling process with different rotation speeds of the agitator shaft for times up to 75 min are presented in Figure 3. We observed a considerable narrowing of the size distributions and a major decrease of the d-values during the first 30 min of the milling process, while the size reduction was much smaller with further increase of the milling time. The milling process was stopped after 75 min, since a further increase of the time did not considerably reduce the particle size or in some cases even resulted in increasing the d-values due to increased particle agglomeration. This is partially observed for the nano-NN-1000 in Figure 3. In addition, long milling times could cause the wear of the zirconia beads and subsequent contamination of the powder and should therefore be avoided. The optimal conditions for the milling were identified to be the rotation speed of 2000 rpm and the milling time of around 75 min.

The $NaNbO_3$ nanopowders, milled for 75 min, were investigated by FE-SEM (Figure 4). The primary particle size was below 100 nm in all samples, and the images confirm the decrease of the particle size with increased rotation speed. In addition, some larger particles of around 200–400 nm could be observed; however, it was not clear, if they were agglomerates or particles. The amount of large particles decreased with increasing rotation speed.

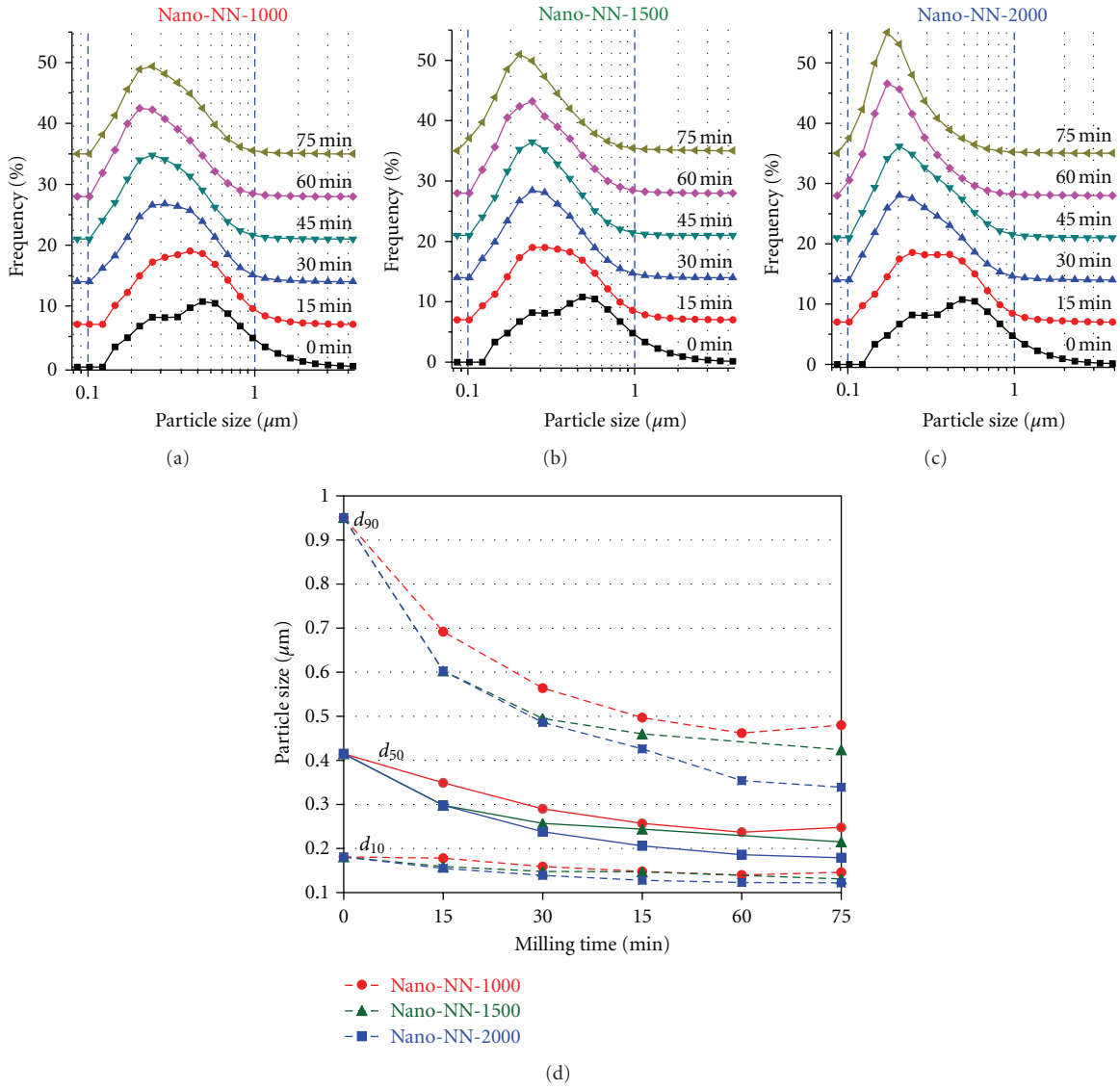

FIGURE 3: The effect of different rotation speeds of the agitator shaft on the milling process of $NaNbO_3$ powders: 1000 rpm (nano-NN-1000), 1500 rpm (nano-NN-1500), and 2000 rpm (nano-NN-2000).

The specific surface areas of the powders, milled for 75 min at different rotation speeds, were measured by the N_2 adsorption method. The results are summarized in Figure 5. The reference-NN powder had the specific surface area of 5.81 m^2/g. After the 1000 rpm milling, the specific surface area increased for about 6 times, while the milling with 2000 rpm resulted in nanopowder with an almost 10 times larger specific surface area. In addition, the d_{BET} primary particle sizes, calculated by (1), are added to Figure 5. The primary particle sizes decrease from 41 nm to 25 nm with increasing rotation speed, which is in agreement with the FE-SEM observations (Figure 4). The particle size of the obtained nano-NN powders is within the ranges reported for solution methods [10–12] and mechanochemical synthesis [13].

The compaction behaviour of the reference-NN and the nano-NN-2000 powders is presented in Figure 6 in the form of a compaction-response diagram [17]. The curve of the reference-NN has a constant slope throughout the whole investigated isostatic pressure range between 250 MPa and 740 MPa, where the highest relative density of about 69% was obtained. A different compaction behaviour was observed in the case of the nano-NN-2000 powder, where lower relative densities were obtained in the lower pressure region up to about 550 MPa; however, a steeper slope, revealing a better compactability of this powder, resulted in higher relative densities at pressures above 550 MPa, as compared to the reference-NN powder. The interpolated value of around 64% relative density at 450 MPa for the nano-NN-2000 powder is comparable to the value reported for the compaction of the solution-derived $NaNbO_3$ nanopowder by Lanfredi et al., that is, 65% at a uniaxial pressure of 450 MPa [11]. However, the authors reported that this relative density was the limiting value, since the compaction rate at pressures above 320 MPa

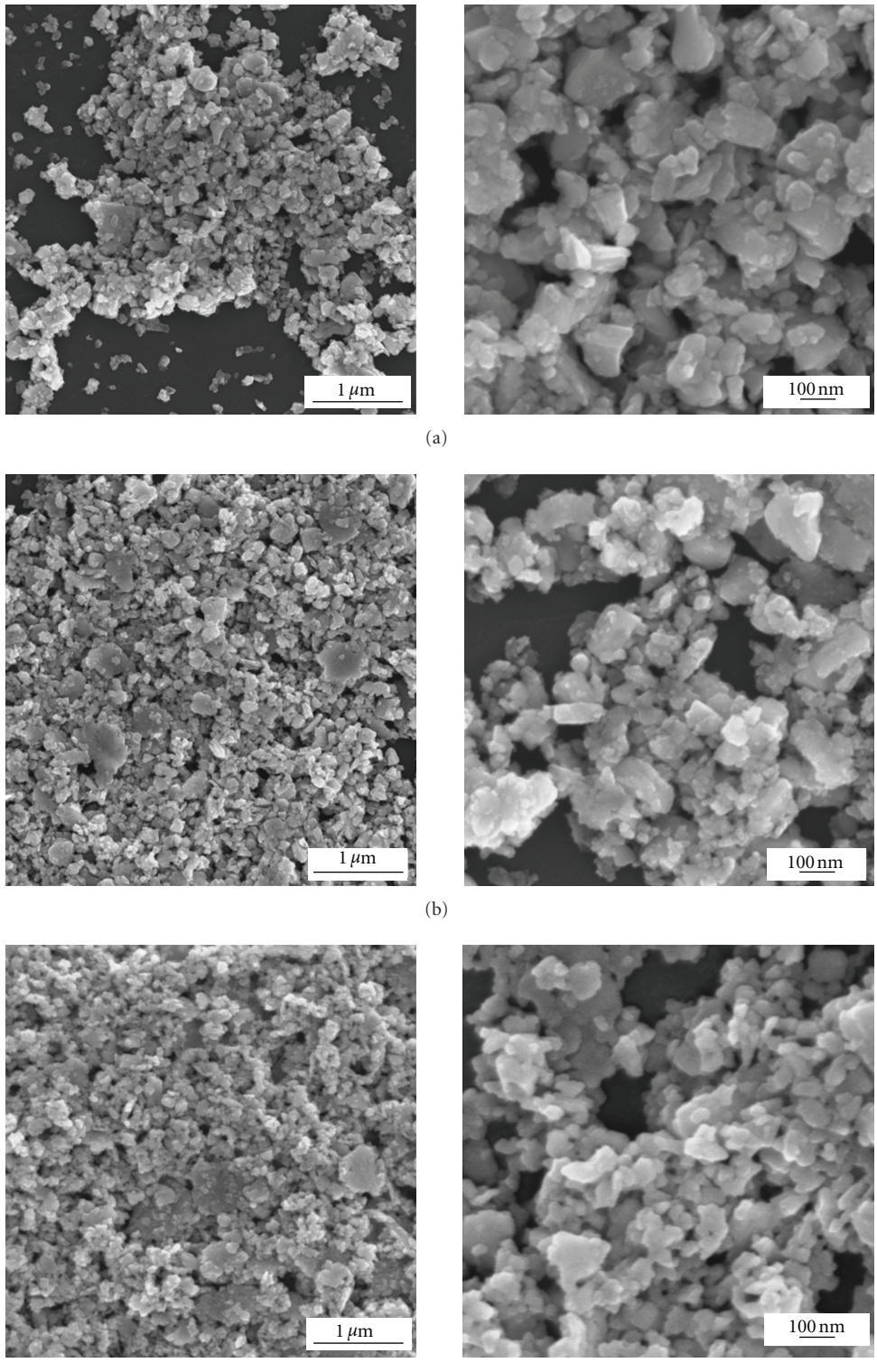

Figure 4: FE-SEM images of the nano-NN-1000 (a), nano-NN-1500 (b), and nano-NN-2000 (c) powders.

was very small. In our case, the limiting value seems to be at higher pressures, since a considerable increase of the relative density was observed with increasing the pressure up to about 650 MPa, where a relative density of around 69.2% was measured. The highest relative density of about 70.2% was achieved at the pressure of 740 MPa.

The pore size and size distribution within the green body are important parameters of the sintering process,

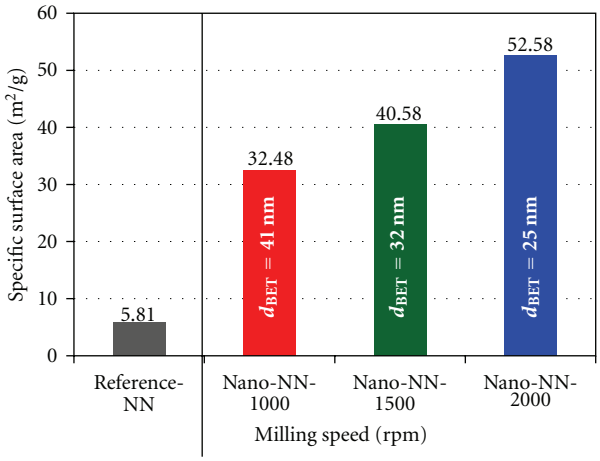

Figure 5: Specific surface areas of the obtained nano-NN-1000, nano-NN-1500, and nano-NN-2000 powders, as measured by the BET method. The calculated d_{BET} values are included in the corresponding columns. The specific surface area of the reference-NN powder is added for comparison.

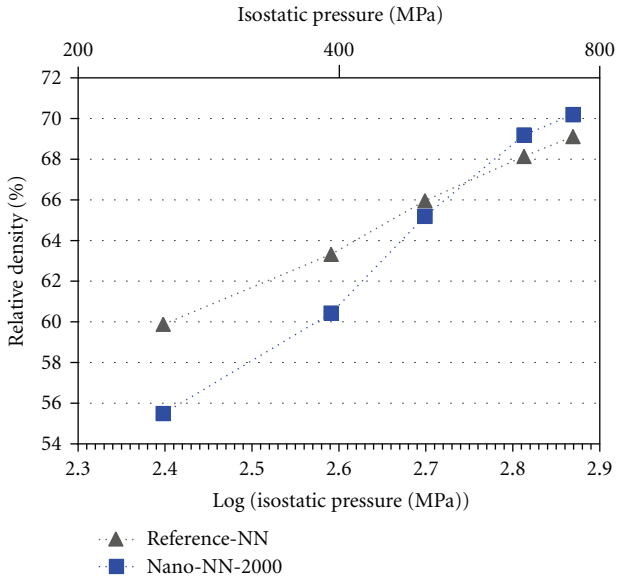

Figure 6: The compaction-response diagram of the reference-NN and nano-NN-2000 powders. Note that the dotted lines are a guide for the eye only.

and, clearly, a uniform pore size distribution is a reflection of a uniform packing of particles, which should promote sintering and densification [18]. The pore size distributions of the reference-NN and nano-NN-2000 green samples, compacted with the pressure of 740 MPa, were determined using the N_2 desorption curves and are presented in Figure 7. The average pore radius is reduced from about 24 nm to about 4 nm, for the reference-NN and the nano-NN-2000 compacts, respectively. Moreover, a much narrower pore size distribution was obtained in the latter case. It is also

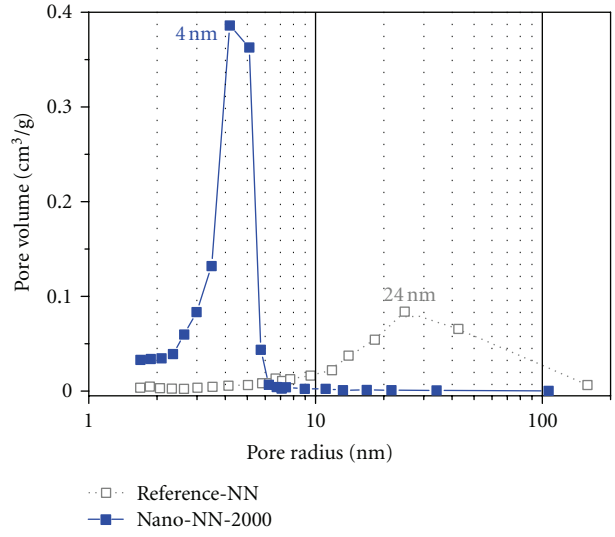

Figure 7: Pore size distribution of the reference-NN and nano-NN-2000 green samples, compacted with an isostatic pressure of 740 MPa. The numbers above the distributions represent the average pore radius.

important to note that both distributions were unimodal, since only one peak was observed in each distribution up to the detection limit of this method, which is at a pore diameter of 400 nm [19]. This could indicate the absence of agglomerates in these green samples; however, further analysis should be performed to confirm this. The fracture surfaces of the two samples, shown in Figure 8, reveal an obvious particle size decrease obtained by efficient bead milling. A detailed study of the sintering behaviour of the nanopowder is in progress.

4. Summary

$NaNbO_3$ nanopowder was prepared by simple top-down processing, combining the solid-state synthesis and subsequent bead milling. The milling process was optimized to yield nanoparticles with the average size of around 25 nm, which is comparable to the particle sizes obtained by solution-based chemical routes or mechanochemical synthesis. The proposed approach does not require any expensive reactants or high-energy milling and, as it is easily upscaled, it could yield a large quantity of the $NaNbO_3$ nanopowder. The compaction behaviour of the nanopowder was investigated in order to establish a suitable starting point for further research of the sintering process. The $NaNbO_3$ nanopowder exhibited a better compactability than the submicron $NaNbO_3$ powder, with an about six times lower average pore radius, and a narrower pore size distribution in the green samples.

Acknowledgments

The authors would like to thank Brigita Kužnik, Katarina Korenčan, Edi Kranjc, and Gregor Trefalt. This work was

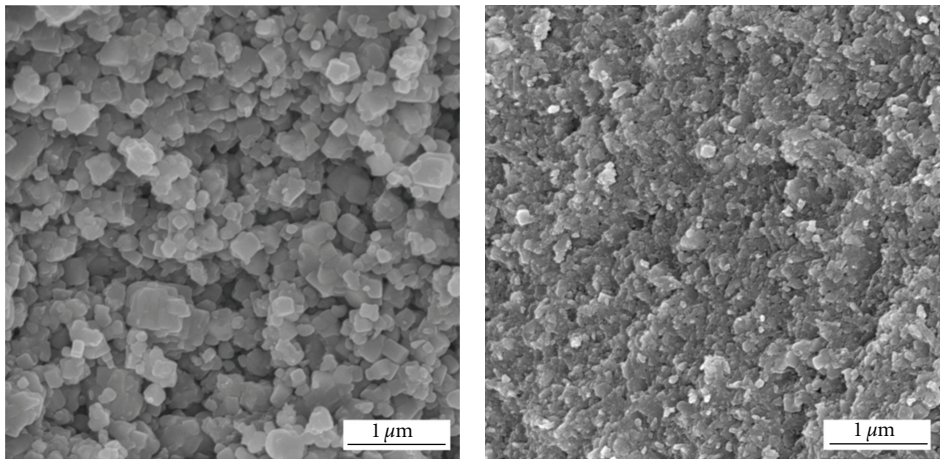

(a) (b)

Figure 8: FE-SEM images of the fracture surfaces of the green compacts pressed with a pressure of 740 MPa: (a) reference-NN, (b) nano-NN-2000.

supported by the Slovenian Research Agency, under Grant no. 1000-08-310121, P2-0105, and J2-1227, and the Centre of Excellence NAMASTE under the Project RRP6.

References

[1] N. H. Fletcher, A. D. Hilton, and B. W. Ricketts, "Optimization of energy storage density in ceramic capacitors," *Journal of Physics D*, vol. 29, no. 1, pp. 253–258, 1996.

[2] W. Y. Pan, C. Q. Dam, Q. M. Zhang, and L. E. Cross, "Large displacement transducers based on electric field forced phase transitions in the tetragonal $(Pb_{0.97}La_{0.02})(Ti,Zr,Sn)O_3$ family of ceramics," *Journal of Applied Physics*, vol. 66, no. 12, pp. 6014–6023, 1989.

[3] G. Shirane, E. Sawaguchi, and Y. Takagi, "Dielectric properties of lead zirconate," *Physical Review*, vol. 84, no. 3, pp. 476–481, 1951.

[4] H. Liu and B. Dkhil, "A brief review on the model antiferroelectric $PbZrO_3$ perovskite-like material," *Zeitschrift fur Kristallographie*, vol. 226, no. 2, pp. 163–170, 2011.

[5] E. P. a. t. E. Council, "Directive 2011/65/EU on the restriction of the use of certain hazardous substances in electrical and electronic equipment," in *Directive 2011/65/EU*, E. Union, Ed., p. 23, Official Journal of the European Union, Strasbourg, France, 2011.

[6] B. Jaffe, W.R. Cook Jr., and H. Jaffe, *Piezoelectric Ceramics*, Academic Press, London, UK, 1971.

[7] H. D. Megaw, "The seven phases of sodium niobate," *Ferroelectrics*, vol. 7, no. 1–4, pp. 87–89, 1974.

[8] Y. Shiratori, A. Magrez, J. Dornseiffer, F. H. Haegel, C. Pithan, and R. Waser, "Polymorphism in micro-, Submicro-, and nanocrystalline $NaNbO_3$," *Journal of Physical Chemistry B*, vol. 109, no. 43, pp. 20122–20130, 2005.

[9] J. Koruza, J. Tellier, B. Malič, V. Bobnar, and M. Kosec, "Phase transitions of sodium niobate powder and ceramics, prepared by solid state synthesis," *Journal of Applied Physics*, vol. 108, no. 11, Article ID 113509, 2010.

[10] M. A. L. Nobre, E. Longo, E. R. Leite, and J. A. Varela, "Synthesis and sintering of ultra fine $NaNbO_3$ powder by use of polymeric precursors," *Materials Letters*, vol. 28, no. 1-3, pp. 215–220, 1996.

[11] S. Lanfredi, L. Dessemond, and A. C. Martins Rodrigues, "Dense ceramics of $NaNbO_3$ produced from powders prepared by a new chemical route," *Journal of the European Ceramic Society*, vol. 20, no. 7, pp. 983–990, 2000.

[12] C. Pithan, Y. Shiratori, J. Dornseiffer, F. H. Haegel, A. Magrez, and R. Waser, "Microemulsion mediated synthesis of nanocrystalline $(K_x,Na_{1-x})NbO_3$ powders," *Journal of Crystal Growth*, vol. 280, no. 1-2, pp. 191–200, 2005.

[13] T. Rojac, M. Kosec, B. Malič, and J. Holc, "Mechanochemical synthesis of $NaNbO_3$," *Materials Research Bulletin*, vol. 40, no. 2, pp. 341–345, 2005.

[14] J.-I. 01-082-0606, *PCPDFWin, PDF-ICDD*, International Center for Diffraction Data, 2002.

[15] J. S. Reed, *Principles of Ceramics Processing*, John Wiley & Sons, New York, NY, USA, 1995.

[16] E. P. Barrett, L. G. Joyner, and P. P. Halenda, "The determination of pore volume and area distributions in porous substances. I. Computations from nitrogen isotherms," *Journal of the American Chemical Society*, vol. 73, no. 1, pp. 373–380, 1951.

[17] R. L. K. Matsumoto, "Generation of powder compaction response diagrams," *Journal of the American Ceramic Society*, vol. 69, no. 10, pp. C246–C247, 1986.

[18] M. N. Rahaman, *Ceramic Processing and Sintering*, Marcel Dekker, New York, NY, USA, 2003.

[19] T. Allen, *Particle Size Measurement: Surface Area and Pore Size Determination*, Chapman & Hall, London, UK, 1997.